CORRECTED 15 APRIL 2025; SEE LAST PAGE
SCIENCE ROBOTICS | RESEARCH ARTICLE

SENSORS

Conductive block copolymer elastomers and psychophysical thresholding for accurate haptic effects

Rachel Blau[1]†, Abdulhameed Abdal[1,2]†, Nicholas Root[3], Alexander X. Chen[1], Tarek Rafeedi[1], Robert Ramji[1], Yi Qie[1], Taewoo Kim[1], Anthony Navarro[1], Jason Chin[1], Laura L. Becerra[4], Samuel J. Edmunds[4], Samantha M. Russman[4], Shadi A. Dayeh[4], David P. Fenning[1], Romke Rouw[3], Darren J. Lipomi[1]*

Electrotactile stimulus is a form of sensory substitution in which an electrical signal is perceived as a mechanical sensation. The electrotactile effect could, in principle, recapitulate a range of tactile experience by selective activation of nerve endings. However, the method has been plagued by inconsistency, galvanic reactions, pain and desensitization, and unwanted stimulation of nontactile nerves. Here, we describe how a soft conductive block copolymer, a stretchable layout, and concentric electrodes, along with psychophysical thresholding, can circumvent these shortcomings. These purpose-designed materials, device layouts, and calibration techniques make it possible to generate accurate and reproducible sensations across a cohort of 10 human participants and to do so at ultralow currents (≥6 microamperes) without pain or desensitization. This material, form factor, and psychophysical approach could be useful for haptic devices and as a tool for activation of the peripheral nervous system.

INTRODUCTION

The most common haptic effects one encounters in consumer devices are produced by mechanical actuators. The primary function of such devices is to deform the skin to produce various tactile cues, such as buzz, rumble, and click. Although the sensations produced using these methods are compelling and reproducible, the gamut is highly limited. Ideally, haptic feedback for human-machine interfaces—for example, for education, entertainment, health care, and medical devices—should be able to produce a much wider range of tactile cues (*1*–*4*). Haptics have become indispensable for consumer devices, such as "vibration mode" on a phone. Similarly, patient engagement and usability devices envisioned for stretchable, epidermal sensors could be substantially deepened with this type of unobtrusive cue. Moreover, use cases for epidermal appliances in physical therapy, robot-assisted surgery, and remote operation could be expanded if they could provide haptic feedback.

All tactile sensations that are ultimately perceived by the brain originate as action potentials in afferents of the peripheral nervous system. Thus, it is in principle possible to generate any tactile percept by activating the relevant set of mechanosensory neurons. Transcutaneous electrical stimulation of the mechanoreceptors using electrodes pressed to the skin has thus held promise for many decades for applications such as haptics, pain relief, and neuroprostheses (*5*). This electrotactile effect is thus a form of "sensory substitution" in which electrical signals can be perceived as mechanical forces (*6*). However, electrotactile stimulation as a means of generating haptic effects has been criticized for many reasons (*7*). It is nonselective, meaning that it produces a range of sensations that are inconsistent between users. This inconsistency is due to differences in skin morphology, unequal hydration, and other parameters that affect contact impedance with the electrodes (*8*). Moreover, high currents and voltages required when using conventional materials (such as metals) and device layouts (like hard planar substrates) also lead to unwanted effects, such as galvanic reactions at the skin surface, pain, and temporary desensitization (*9*). Also, the area of stimulation tends to be large, and electrical signals have the potential to stimulate the muscles and the mechanosensors (*10*).

Nevertheless, the toolkits of materials chemistry, microfabrication engineering, and signal detection theory applied to cognitive science have the potential to increase the realism, safety, and reliability of electrotactile effects (*11*). Such development would greatly enable haptic effects in epidermal circuits, where devices in wearable form factors would otherwise have to be made thicker to accommodate components with moving parts (*12*–*15*). Here, we used an integrated materials design strategy that combines a purpose-synthesized, stretchable, conductive block copolymer; concentric electrodes in a stretchable layout; and a psychophysical design strategy for consistent stimulation of mechanical sensations in human participants (*8*, *16*, *17*). Using these tools and a large dataset, we were able to show extraordinarily low stimulation currents (≥6 μA), improved spatial localization, greater acuity by the participant, and the ability to toggle between sensations characterized as pressure or vibration by modifying the frequency of the signal.

RESULTS

Synthesis of intrinsically stretchable PEDOT-based one-component electrode

Our strategy is illustrated in Fig. 1. The material (Fig. 1A) is a conductive block copolymer based on the well-known polyelectrolyte complex poly(3,4-ethylenedioxythiophene):poly(styrenesulfonate) (PEDOT:PSS). To circumvent the stiffness and brittleness of pristine PEDOT:PSS, which does not make conformal coverage with the uneven surface of the skin, we used a block copolymerization strategy

[1]Aiiso Yufeng Li Family Department of Chemical and Nano Engineering, University of California, San Diego, La Jolla, CA, USA. [2]Department of Mechanical and Aerospace Engineering, University of California, San Diego, La Jolla, CA, USA. [3]Brain and Cognition, Psychology Department, University of Amsterdam, Amsterdam, Netherlands. [4]Department of Electrical and Computer Engineering, University of California, San Diego, La Jolla, CA, USA.
*Corresponding author. Email: dlipomi@ucsd.edu
†These authors contributed equally to this work.

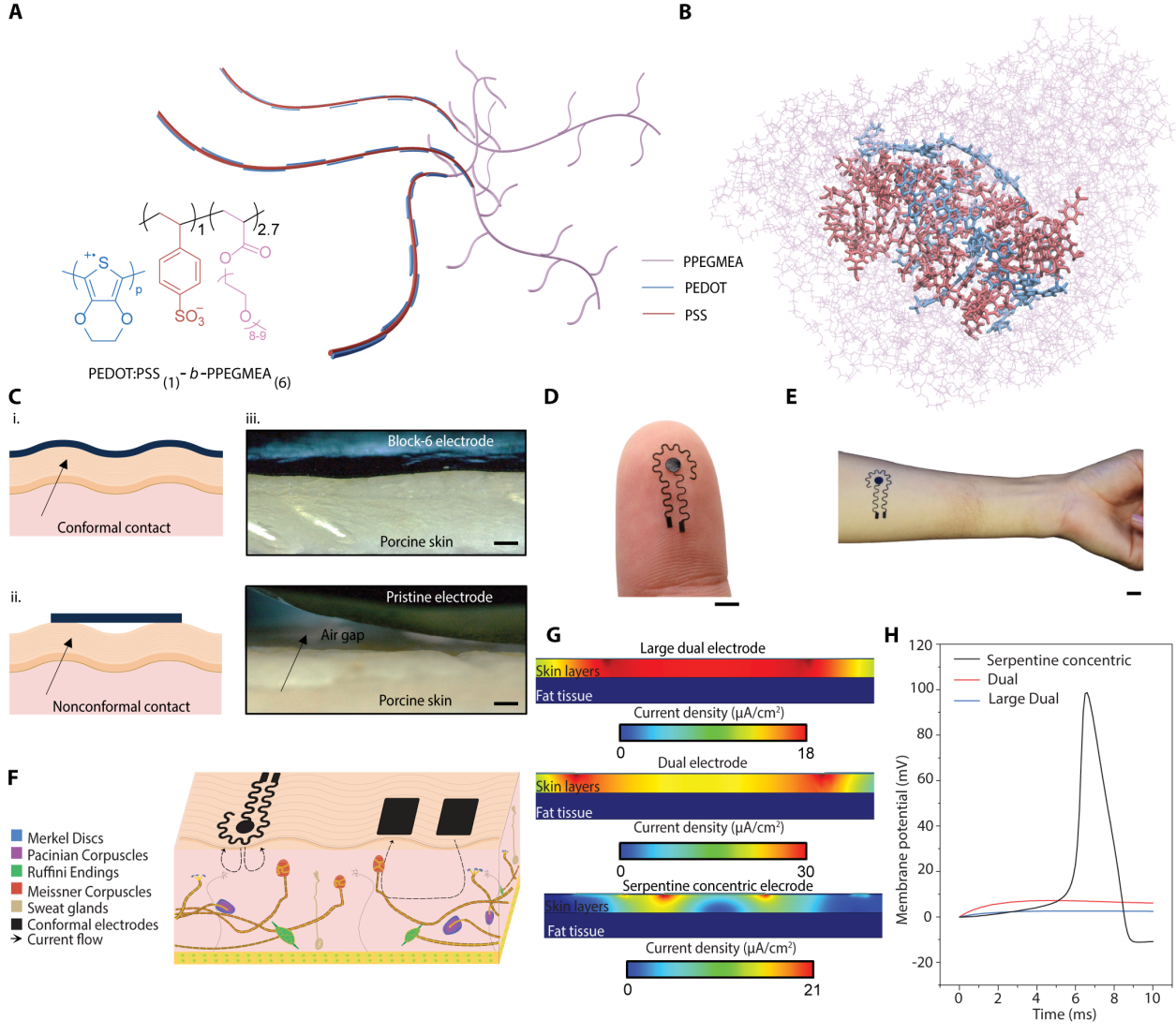

Fig. 1. Intrinsically stretchable organic and soft electrode for electrotactile applications. (**A**) Schematic illustration of the intrinsically stretchable PEDOT derivative known as Block-6. (**B**) Atomistic molecular dynamics simulation of Block-6. (**C**) Schematic illustration of (i) Block-6 and (ii) pristine PEDOT:PSS conformability on corrugated skin. (iii) High-resolution optical images displaying conformability of the electrode on porcine skin at ×200 magnification. Scale bar, 100 μm. (**D** and **E**) Photographic images of conformal and stretchable concentric electrodes on human skin for electrotactile applications, including the fingertip (D) and the forearm (E). Scale bars, 1 mm and 1 cm, respectively. (**F**) Schematic illustration showing the comparison of current flow in serpentine concentric and dual electrode designs. (**G**) Simulation results of current density distribution in dual and serpentine concentric electrodes. The large electrode has a contact area of 2217 mm^2. The dual and serpentine electrodes have comparable contact areas of 505 and 509 mm^2, respectively. (**H**) The Hodgkin-Huxley model shows nerve actional potential triggered in serpentine concentric electrode design as a result of localized current density.

described recently by our group (*18*, *19*). The goal was to make a low-impedance conductive polymer with a high degree of mechanical deformability that can be patterned easily into conductive traces. Briefly, a flexible bottlebrush segment based on poly(poly(ethylene glycol) methyl ether acrylate) (PPEGMEA) was covalently bound to the PSS chain using the reversible addition-fragmentation transfer (RAFT) process, a type of quasi-living controlled radical polymerization. The resulting polymer was termed PEDOT:$PSS_{(1)}$-*b*-$PPEGMEA_{(6)}$ ("Block-6"), where the subscripts refer to the mass ratios of the two segments (figs. S1 to S5). Inclusion of the large, flexible units resulted in a much lower elastic modulus than that of PEDOT:PSS (~10 MPa compared with ~380 MPa) (*18*). A molecular dynamics simulation of a single polymer chain with associated PEDOT (Fig. 1B) revealed the flexible PPEGMEA chains surrounding the stiffer PEDOT:PSS core, reminiscent of common thermoplastic block copolymer elastomers such as poly(styrene-butadiene-styrene) (SBS). The low elastic modulus of Block-6 allowed for notably greater conformal contact on the surface of the skin (Fig. 1C and fig. S6). Poor contact leads to increased impedance, larger currents, and greater chance of pain upon stimulation (*20*, *21*).

Electrode design and fabrication

Using laser ablation, we fabricated a design consisting of concentric electrodes in a serpentine layout (Fig. 1, D and E). Although the addition of

serpentine microstructures may not be groundbreaking, integrating them into our intrinsically stretchable material offers notable advantages. Our material inherently stretched up to approximately 10% elastically, and the incorporation of serpentine microstructures extended its stretchability, making it suitable for use as a skin interface. The details of fabrication are given in figs. S7 to S10. Briefly, the Block-6 electrodes were deposited atop a thin film of poly(methyl methacrylate) (PMMA) on a stretchable substrate, polydimethylsiloxane (PDMS). We chose to test for tactile effects on the forearm because it represented a greater challenge for controlled tactile effects compared with the fingers, which have a lower stimulation threshold and a higher afferent density (*22*–*24*).

Recent studies indicate that a range of current densities (0.1 to 10 mA cm^{-2}) can stimulate sensory fibers residing at the epidermis-dermis junction (*7*). In addition, the distribution of the low current density should be localized to activate nearby mechanoreceptors (and not muscles). Thus, to stimulate locally, a concentric design was adopted for the ventral forearm (Fig. 1, E and F, and figs. S11 and S12). A finite element analysis (FEA) simulation showed that the current density distribution was localized across the skin layers as opposed to monopolar designs of a similar area (~10 cm^2) and current source (10 μA) (Fig. 1G and fig. S13). The electrode dimensions were optimized to fit the forearm, and the current applied was the average detection threshold from the participants (~10 μA) (fig. S13). The electronic properties used for current density simulations are shown in fig. S14 and table S1. We assessed the effectiveness of current density distribution on an embedded nerve fiber in the epidermis layer by implementing the Hodgkin-Huxley model, which describes action potential propagation (table S2). Schematics illustrating the nerve fiber location and embedment in the dermis are shown in figs. S15 and S16. The model suggests that the action potential only propagates along the fiber when a concentric design is placed on the skin, given that it remains untriggered in a conventional electrode because of the nonlocalized current spread (Fig. 1H and fig. S17). Furthermore, we conducted an evaluation of the dual electrode with a total contact size (505 mm^2) comparable to that of serpentine concentric (509 mm^2) and gap distances of 20 and 9 mm, as depicted in fig. S13. This assessment revealed an increase in current density compared with the larger dual electrode, and it triggered an action potential at a 9-mm gap distance (fig. S18). However, the gap distance is usually 20 to 50 mm for dual electrodes (*25*). Existing reports generally favor the use of larger electrodes to minimize the likelihood of inducing painful sensations (*26*). Consequently, the geometric shape that we used influences the magnitude of the current stimulation and the subsequent sensation.

Characterization of Block-6 as a haptic interface

The electrochemical characteristics of the Block-6 electrode influence how charge is transported across the electrode/skin junction. For example, the capacitance of the electric double layer (EDL) within a conductive polymer determines the amount of charge that can be injected (*27*, *28*). PEDOT:PSS exhibited capacitive behavior because of the charged sulfonate groups; these charges permit mixed (ionic and electronic) conductivity (Fig. 2A and fig. S19A) (*29*). The cyclic voltammetry (CV) of Block-6 showed capacitive behavior by the rectangular shape hysteresis in the voltammogram and the linear dependence of the current with the scan rate (fig. S19B) (*30*). In addition, the electronic function of the electrode is dependent on both the electrical and ionic conductivity of Block-6. Although the electrical conductivity of Block-6 is lower than that of pristine PEDOT:PSS, the PPEGMEA chains promote ionic transport and thus result in a greater EDL capacitance, indicated by a greater slope when measured from CV (fig. S19B) (*29*, *30*). The CV additionally exhibited a larger area compared with pristine PEDOT:PSS, suggesting a larger charge storage capacity of Block-6 (Fig. 2B and fig. S20). Finally, the excursion potential of Block-6 and pristine PEDOT:PSS was measured with a charge injection of 2.08 mA mm^{-2}, and both electrodes showed comparable stability in terms of voltage buildup (Fig. 2C). This is important for safety consideration during charge injection (*31*). However, increasing the injection current resulted in delamination of PEDOT:PSS (fig. S21), whereas the injection current of the Block-6 electrode could be increased to 36 mA (75 mA cm^{-2}) while remaining intact. A critical consideration for wearable electrodes is compatibility with elastic human skin (*32*). Delamination due to mismatch in modulus can result in increased impedance; increased voltage required for simulation; and greater chance of pain, galvanic reactions, and other unwanted effects. The viscoelasticity of Block-6 permits local conformability to the uneven surface of the skin and lateral stretching due to global deformation of the skin (Fig. 2D and fig. S22). Microscopic conformability in particular is unfeasible for high-modulus metallic films (*33*). Here, the concentric Block-6 electrodes were designed to have serpentine structures to accommodate increased elastic strain and reduced changes in interfacial impedance upon stretching (Fig. 2E). In addition, impedance measurements on human skin were lower for Block-6 across all frequency ranges (fig. S23). Mechanical simulations suggested that the elasticity of the freestanding Block-6 electrode was ~44% (figs. S24 and S25). Although the elasticity of the assembled device decreased to ~19% because of the bonded contacts on the elastomeric substrate (fig. S26), this remains a ~3× improvement compared with recent reports of metallic interconnects on elastomers (*34*). Likewise, strain-resistance measurements indicated that the Block-6 electrodes exhibited negligible piezoresistivity, meaning no increase in resistance up to 30% for at least 500 cycles (fig. S27). Also, we characterized the contact resistance between silver and Block-6 (0.217 ohm·cm^2), which is comparable to that between silver and pristine PEDOT:PSS (0.237 ohm·cm^2) (fig. S28). Additionally, simulations suggest that torsion of the electrodes up to 180° results in von Mises stresses that are less than half of the yield strength (Fig. 2G). Finally, the intrinsic stretchability of the polymer coupled with the serpentine design allows the device to achieve strains of 100% before failure (Fig. 2F). The PPEGMEA chains render a lower loss and storage modulus (Fig. 2H and fig. S29), with higher viscoelasticity than that of pristine PEDOT:PSS (figs. S29 and S30). When compared with physical blends involving PEDOT (Fig. 2I), the covalently engineered Block-6 has the lowest modulus, indicating that it is the closest to that of human skin.

Psychophysical thresholding for electrotactile perception

Both electrical and mechanical stimuli can activate nerve fibers that evoke the sense of touch. Mechanical stimulus results in the deformation of mechanoreceptors, whereas electrical signals produce a potential gradient across nerve fibers, resulting in depolarization and repolarization events across the membrane of receptor cells. As a result, these stimuli trigger action potentials that ascend toward the central nervous system (CNS) in the same biological pathway (Fig. 3A) (*35*, *36*). For mechanical stimulus, the type and intensity of the sensation triggered by activation of mechanoreceptors are a function of

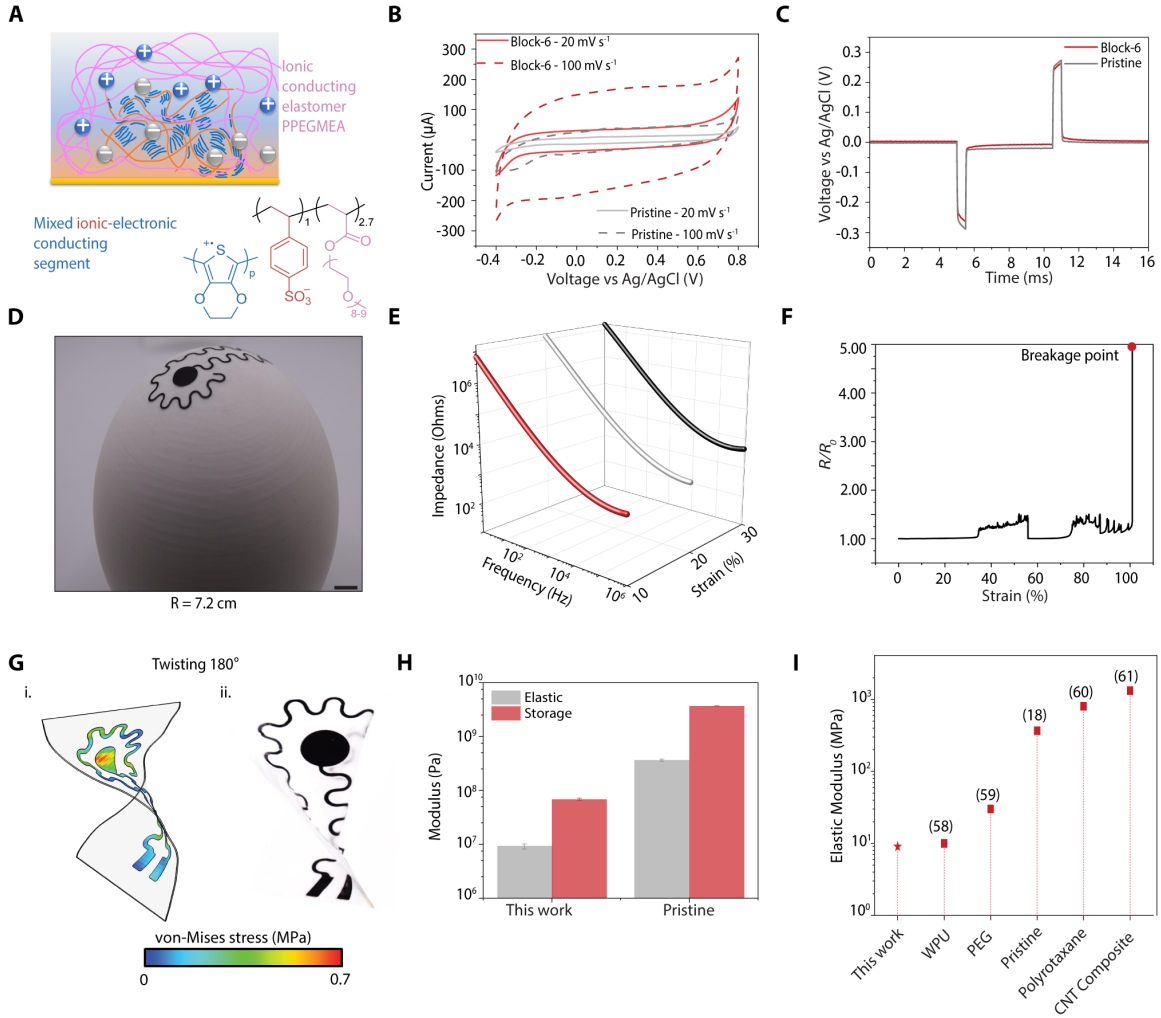

Fig. 2. Electrochemical and electromechanical characterization of conformal electrode. (**A**) Schematic illustration showing the mixed ionic-electronic conductive segment of PEDOT:PSS and the covalently bound ionic conductive elastomer PPEGMEA segment. (**B**) CV scans of Block-6 and pristine PEDOT:PSS from 20 to 100 mV s^{-1} in step increments of 20 mV s^{-1}. (**C**) Comparable voltage buildup during charge injection through the Block-6 and pristine PEDOT:PSS films. (**D**) Photograph of a concentric Block-6 electrode on a spherical surface. Scale bar, 8 mm. (**E**) Interfacial impedance of a concentric Block-6 electrode after different strains illustrating the stability of the conformal dry electrode. (**F**) Change of resistance of Block-6 as a function of strain applied. Fluctuations are due to twisting and buckling until the device is constrained to a unidirectional motion. (**G**) FEA simulations (i) and photograph of device (ii) after twisting 180° resulted in low von Mises stress. (**H**) Comparison of elastic and storage moduli for Block-6 and pristine PEDOT:PSS, showing copolymerization resulting in increased softness and deformability. (**I**) Comparison of elastic modulus of Block-6 as used in this work with PEDOT:PSS and as blended with other polymers (*18*, *59*–*61*) and nanomaterials (*62*).

displacement and frequency. For example, afferents terminating in the Merkel cell–neurite complexes (slow-adapting type I) are responsible for the sensation of sustained pressure, whereas rapid-adapting mechanoreceptors (RAMs) are sensitive to vibrotactile stimulation (*37*). Aβ-fiber RAMs in the hairy skin are tuned to very similar frequencies as those terminating in Meissner corpuscles (rapid-adapting type I) deliver low vibration sensations and are believed to make up part of the sensation of fine textures (*38*, *39*).

To relate the parameters of electrical stimulation to the sensation perceived, we performed psychophysical experiments on a group of participants (Fig. 3B). Safety protocols were assessed before experimenting with stimulation (figs. S31 and S32). We designed a set of psychophysical tests that characterized key elements in electrotactile stimulation, including pain and detection thresholds, perception quality, spatial acuity, and contrast discrimination. Detailed psychophysical tasks and procedures are described in figs. S33 to S35. Furthermore, we have demonstrated that materials like pristine PEDOT:PSS (known for rigidity) and copper (characterized by high impedance) are impractical for electrotactile applications (figs. S36 and S37). The psychophysical evaluations began with pain threshold measurement by applying biphasic current stimulation (10 to 250 μA). Measuring pain thresholds enables us to know whether a participant might feel uncomfortable on subsequent tasks. Fortunately, the highest intended stimulation current for the detection threshold experiment was ~4× lower than the lowest pain threshold of any participant (Fig. 3C). To quantify the detection threshold associated with the haptic sensations invoked, we used a two-alternative forced choice (2AFC) design to measure

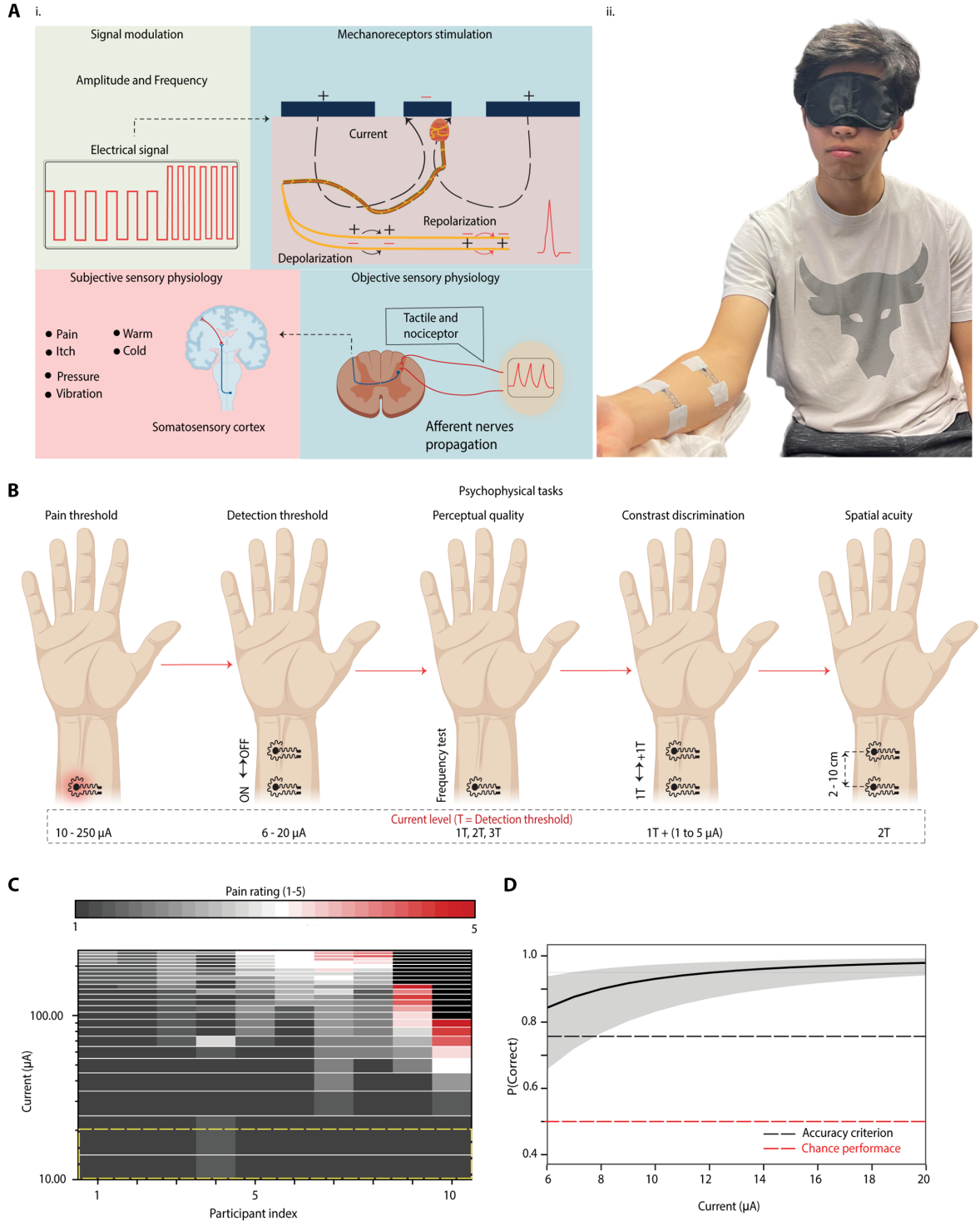

Fig. 3. Experimental setup of psychophysical tasks for electrotactile perception. (**A**) (i) Flow diagram of haptic perception by signal modulation and activation of mechanoreceptors. (ii) Participant performing the psychophysical task. (**B**) Flow diagram of psychophysical tasks performed on the forearm and the current level applied. (**C**) Heatmap of pain threshold (1 to 5) as a function of current from 10 to 250 µA, where the yellow dashed box shows the stimulation window used for the detection threshold ($n = 639$ trials). (**D**) Participant accuracy (y axis) in 2AFC detection task as a function of stimulation current. Red dashed line depicts chance performance. Black dashed line depicts accuracy criterion, and red dashed line depicts chance performance. Data are estimated marginal means of GLMM fixed effect (black line) and 95% CI on fixed effect (shaded gray ribbon), transformed to response scale with inverse logit function ($n = 1280$ trials).

the accuracy with which participants could identify which of two electrotactile devices had been stimulated. Even at the lowest stimulation current of 6 μA, participants' accuracy was notable, reaching 84%, which was significantly higher than would be expected by chance ($P < 0.005$; see the "Statistical analysis" section) and higher than the 75% accuracy criterion classically used to define the sensory detection threshold (Fig. 3D and fig. S38) (*40*). To our knowledge, ≤6 μA is among the lowest sensory detection threshold reported for an epidermal electrotactile device.

Evaluation of the quality of the percept

Idiosyncrasies of the participants, such as differences in skin morphology, hydration, and concentration, can lead to individual differences in sensation (*10*). In subsequent experiments, we accounted for these individual differences by applying a current amplitude equal to (1T), twice (2T), or three times (3T) the detection threshold level for each participant (rather than applying fixed currents across participants). We hypothesized a gamut of percepts by normalizing the stimulation frequency. Across all combinations of frequency and current of electrical stimulation, participants predominantly experienced the sensation of either pressure or vibration. In fewer than 5% of trials, a different sensation was reported [typically itch, possibly because of the activation of pruriceptors (*41*)]. Overall, the participants were significantly more likely to experience vibration at higher frequencies of stimulation and pressure at lower frequencies of stimulation ($P < 0.001$) (Fig. 4A and fig. S39) (*42*). On average, increasing the stimulation frequency by 70% doubled the odds of experiencing vibration versus pressure. Our model predicts that the "crossover" point at which participants first begin to report vibration more often than pressure is ~6 Hz (Fig. 4B). The frequency of the crossover point happens to correspond to the frequency at which Meissner corpuscles (sensitive to low-frequency vibrations) become more sensitive to vibration than Merkel cell–neurite complexes (which typically respond to sustained pressure but are also sensitive to very low–frequency vibrations) (*11*, *43*). Aβ-fiber RAMs in hairy skin are sensitive to frequencies between 10 and 50 Hz, similar to the range that activates fibers terminated in Meissner corpuscles found in glabrous skin (*37*). This observation suggests that the change in conscious sensation from pressure to vibration might reflect an equivalence (in the elicited patterns of neuronal activation) between electric stimulation and mechanical stimulation at a given frequency (Fig. 4C).

Although the type of sensation (pressure versus vibration) was strongly dependent on the frequency, it was not significantly affected by the current ($P > 0.05$). Instead, changes in stimulation current affected the intensity of the sensation perceived, with stronger currents corresponding to a more intense sensation (for instance, doubling the stimulation current increased the perceived intensity by approximately 0.25 on the 1 to 5 intensity scale; fig. S40). As predicted by the pain thresholding, all sensations were reported to be between "very comfortable" and "neutral," except for a single trial for a single participant (who rated the 10-Hz stimulation at detection threshold as "uncomfortable"). Furthermore, almost all sensations (93%) were experienced as localized rather than referred (5%) or radiating (1%). The probability of experiencing a sensation as localized did not significantly depend on frequency or current (both $P > 0.05$; Fig. 4D). Moreover, we have assembled a comprehensive table for comparing our work with the existing literature (table S3).

Spatial acuity and contrast discrimination

Finally, the types of sensation, spatial acuity, and contrast discrimination achievable by electrotactile means depend on the type and density of nerve endings found on various regions of the body. Previous studies suggest that the spatial acuity for the forearm by electrical stimulus (a type of two-point discrimination test) is 9 to 40 mm (*7*, *44*, *45*). Using our materials, we varied the distance between two electrodes from 2 to 10 cm (fig. S41). The smallest distance between electrodes tested was constrained by the outer terminal of the concentric electrode, which had a radius of ~1 cm (figs. S11 and S12). Even at the smallest possible center-to-center distance, 2 cm, participants could identify whether stimulation came from one versus both electrodes with 95% accuracy ($P < 0.001$; fig. S42). Overall, the identification of spatial acuity was significantly higher than chance ($P < 0.001$). There was not a significant relationship between interelectrode distance and acuity accuracy ($P = 0.53$). However, increasing the difference in current between the electrodes at a fixed position (meaning the just noticeable difference) corresponded to better accuracy ($P < 0.001$) (Fig. 4E). On average, increasing the "contrast" in signal by 13% doubled the odds of identifying which site had higher current.

We conducted a comparative analysis of our Block-6 psychophysical results with silver/silver chloride (Ag/AgCl) commercially available electrodes with identical experimental settings (fig. S43A). Hence, it was possible to directly compare the electrodes at different amounts of current delivery. The detection performance at 6 μA was far lower than the accuracy criterion (fig. S43B). Therefore, we increased the current amplitude up to 80 μA for further investigation of the detection threshold (fig. S43C). We found that Block-6 outperforms the commercial electrode and that the minimum current for above-chance performance on the commercial electrode is ~25 μA (~3× higher current than with Block-6). Also, the commercial electrode crossed the traditional psychophysics threshold definition of 75% accuracy at ~40 μA (~5× higher current than ours). Moreover, the frequency modulation resulted in more thermal and itching sensations (fig. S43D). The toggling effect between pressure and vibration was imperceptible with this type of electrode. Last, the dual electrode experienced more current spread, and thus, the response proportion was not localized at all frequencies (fig. S43E).

DISCUSSION

The generation of haptic effects by direct electrical stimulation of afferent fibers has held promise as a means of sensory substitution. Here, we have shown how an integrated strategy that includes polymer engineering, device layout, and psychophysical thresholding based on signal detection theory can be used to overcome the occurrence of pain, desensitization, lack of realism, and participant-to-participant variation, which have previously hindered this technique. These methods allow delivery of ultralow stimulation currents with high spatial precision. We also demonstrated the ability to toggle between sensations categorized by participants as pressure and those categorized by participants as vibration by adjusting the frequency of electrical stimulation. Moreover, the crossover point in electrical frequency at which perception of vibration is more likely than perception of pressure is similar to the mechanical frequency at which Aβ-fiber RAMs, a subset of low-threshold mechanoreceptor activated by low-frequency vibrations, become more sensitive than Merkel afferents. This observation suggests an equivalency between electrical and mechanical stimulation. The ability to bypass the mechanically

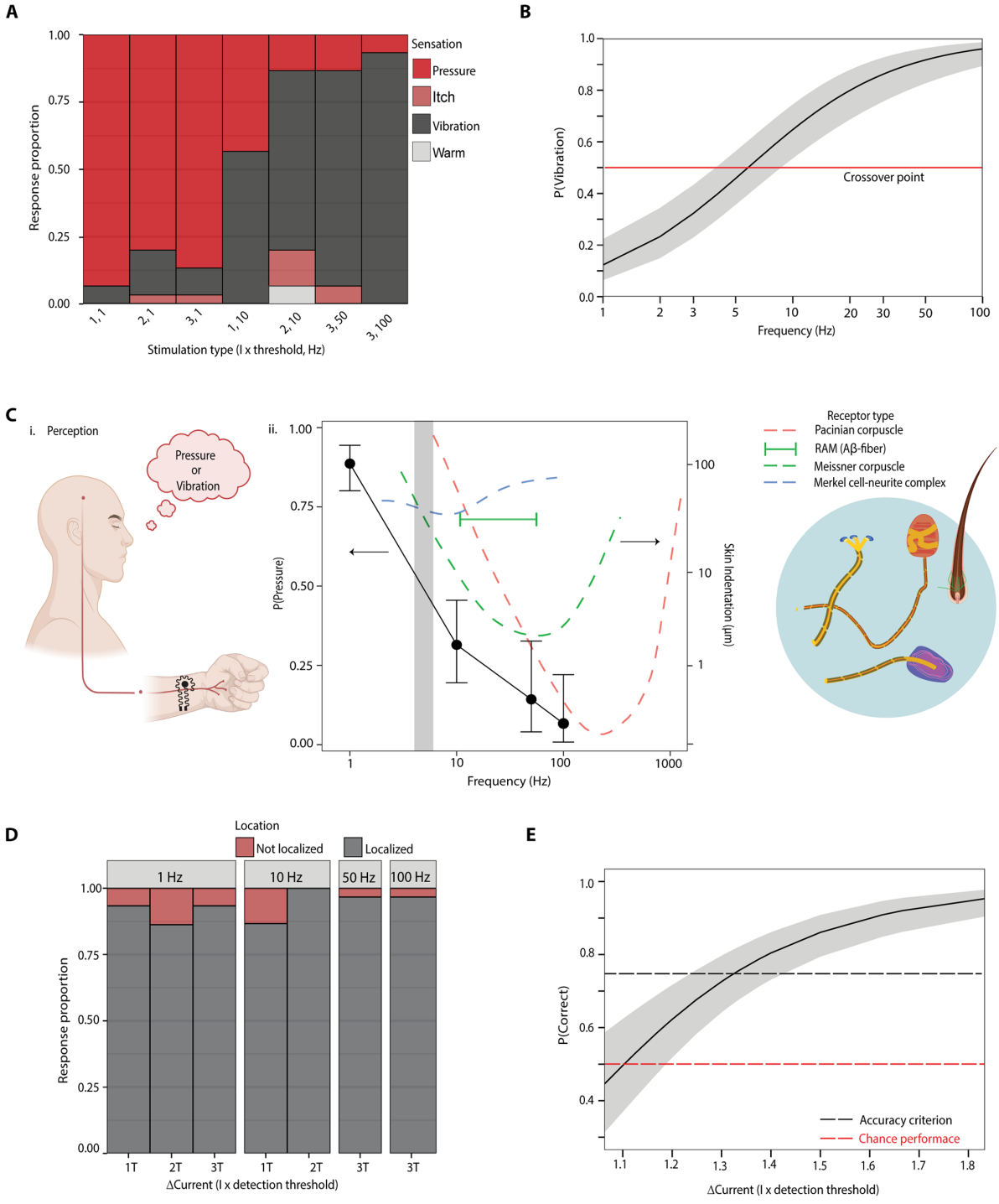

Fig. 4. Psychophysical experiments of sensation perception, localization, and contrast discrimination. (**A**) Proportion of the time a stimulus was judged as pressure, itch, warm, or vibration (*y* axis) as a function of type of stimulation (*x* axis). Stimulation type was a combination of stimulation frequency (Hz) and stimulation current (multiple of the participant's detection threshold) ($n = 210$ trials). (**B**) Model of the probability of reporting vibration versus pressure (*y* axis) as a function of stimulation frequency (*x* axis; Hz). Red line depicts crossover point. Data are estimated marginal means of GLMM fixed effect (black line) and 95% CI on fixed effect (shaded gray ribbon). (**C**) (i) Schematic illustration of the participants perceiving different sensations. (ii) Response proportion for pressure normalized by frequency (black line) and compared with receptor temporal sensitivity (red, green, and blue dashed lines). The gray highlight shows the crossover point at ~6 Hz overlaying the sensitivity of Meissner corpuscle and Merkel cells. The green horizontal line shows the range of frequencies for sensitivity to vibration of Aβ-fiber RAMs on hairy skin. Error bars are 95% CIs on binomial proportion (Clopper-Pearson method), from $N = 30$ participants (200 trials total). (**D**) Participant response to localization as a function of threshold and frequency ($n = 210$ trials). (**E**) Participant accuracy (*y* axis) in 2AFC discrimination task as a function of difference in stimulation current. Red dashed line depicts chance performance, and black dashed line depicts classic accuracy criterion for sensory detection. Data are estimated marginal means of GLMM fixed effect (black line) and 95% CI on fixed effect (shaded gray ribbon) ($n = 400$ trials).

sensitive apparatus and activate the appropriate neurons transcutaneously could be valuable not only in haptics but also in neural prostheses.

We note that several observations in this study may open new avenues for research. For example, our results hinted at the possibility of a type of tactile contrast: increased discrimination when different electrical signals were supplied by adjacent electrodes. This capability could be highly valuable in the development of tactile displays, human-machine interfaces, accessibility devices, or new forms of artwork, especially for the blind. Furthermore, the results from our cohort in which participants categorized a small number of electrotactile stimuli as "itch" or "heat" (in addition to the dominant categories of pressure and vibration) suggest a broader gamut of tactile percepts to the electrotactile effect than may have been previously known. Such results also hint at the ability to achieve multimodal stimulation given a more complex waveform or juxtaposition of electrodes providing different signals.

Finally, we note that the technical sophistication of our electrode setup is not the best that can possibly be achieved. The excellent work of many investigators in the field of epidermal electronics has demonstrated stretchable layouts with greater resolution than that reported here. More sophisticated layouts with multiplexed outputs and tighter resolution, combined with the materials and psychophysical calibration reported here, may still lead to new capabilities.

MATERIALS AND METHODS

Number-average molecular weight (M_n), weight-average molecular weight (M_w), and dispersity (D') were determined using an Agilent Technologies 1260 Infinity II LC system. The mobile phase was 30% methanol and 70% 0.2 M sodium nitrate ($NaNO_3$) and 0.01 M monosodium phosphate (NaH_2PO_4) in water at pH 7 (adjusted with concentrated sodium hydroxide, NaOH) at 40°C at 1 ml min^{-1}. The PL aquagel-OH Mixed-B column, calibrated against narrow dispersity PSS standards (purchased from Polymer Standards Service), was used. ^{1}H nuclear magnetic resonance (NMR) spectra were acquired in deuterium oxide, D_2O, at room temperature on a Bruker AVANCE III 600 MHz NMR spectrometer fitted with a 1.7-mm triple resonance probe with the z-gradient.

Materials

Sodium 4-styrenesulfonate (NaSS), 4,4′-azobis(4-cyanovaleric acid) (ACVA), azobis(isobutyronitrile) (AIBN), PEGMEA (M_n = 480 g mol^{-1}), 4-cyano-4-(phenylcarbonothioylthio)pentanoic acid (the RAFT chain transfer agent), and ethylenedioxythiophene (EDOT) were purchased from Sigma-Aldrich and used without further purification. Distilled water filtered using a Milli-Q purification system was used throughout.

Synthesis of PEDOT:PSS$_{(1)}$-*b*-PPEGMEA$_{(6)}$ (Block-6)

RAFT polymerization of PSS$_{(1)}$-b-PPEGMEA$_{(6)}$ block copolymer

PSS$_{(1)}$-*b*-PPEGMEA$_{(6)}$ was synthesized as previously described (*18*). Briefly, PSS macro-RAFT was synthesized by RAFT polymerization of NaSS monomers. The RAFT agent was 4-cyano-4-(phenylcarbonothioylthio)pentanoic acid, and the initiator was ACVA. The reaction ratio was 0.2:1:150 initiator:RAFT agent:monomers. The reaction was stopped by exposure to air. PSS macro-RAFT was purified by precipitation in acetone and dried under vacuum to afford a pink powder. Next, to synthesize the PSS-*b*-PPEGMEA, we used the previously synthesized PSS macro-RAFT along with the ACVA initiator and PEGMEA monomers and carried out a second RAFT polymerization. The reaction ratio was 0.2:1:400 [initiator]:[PSS macro-RAFT agent]:[monomers]. The ^{1}H NMR of the crude mixtures showed 93% PEGMEA conversion.

Synthesis of PEDOT: PSS$_{(1)}$-b-PPEGMEA$_{(6)}$ (Block-6)

PEDOT:PSS$_{(1)}$-*b*-PPEGMEA$_{(6)}$ was synthesized as previously reported (*18*). Briefly, PSS$_{(1)}$-*b*-PPEGMEA$_{(X)}$ was dissolved in Milli-Q water at a concentration of 75 mg ml^{-1} and was acidified by Dowex Marathon C hydrogen form for 18 hours. The polymer solution was filtered over a 10-μm filter. Sodium persulfate (1150 mg, 4.83 mmol) and iron trichloride (100 wt % in water, 0.175 ml) were added to the filtrates of 4875 mg of PSS$_{(1)}$-*b*-PPEGMEA$_{(6)}$, 65 ml. The solution was vigorously stirred before the addition of EDOT (500 mg, 3.51 mmol). Milli-Q water was added in small portions to prevent gelation. The final volume was 180 ml. The reaction was left to react for 24 hours at room temperature. PEDOT:[PSS$_{(1)}$-*b*-PPEGMEA$_{(6)}$] was purified by stirring over acidic resin (Dowex Marathon C hydrogen form, 17 g) and basic resin (Lewatit MP-62 free base, 11 g) for 6 hours, followed by a 10-μm filtration.

Fabrication of the Block-6 film

A custom mold made from clear V4 resin was three dimensionally (3D) printed (Form 3+) with a thickness of 0.5 mm for drop casting. The mold was sonicated with isopropyl alcohol (IPA), acetone, and deionized (DI) water sequentially and then dried with nitrogen (N_2) gas. Mold release (Ease Release 200, Mann Release Technologies) was sprayed on the 3D-printed mold and left to dry at room temperature. Block-6 ink was vigorously stirred and degassed for at least an hour before drop casting. A disposable plastic syringe (1 ml, Henke-Ject) was used to disperse 6.5 ml of the solution. The film was dried on a hot plate covered with a Pyrex tray at 65°C for 1 hour and 30 min. The film thickness was measured with a profilometer (~20 μm, Bruker Dektak XT stylus). The film was peeled using tweezers and stored in a plastic storage container.

Psychophysics procedure and statistical analysis

Participant recruitment and safety protocol assessment

The experimental protocol was approved by the Internal Review Board at the University of California (UC) San Diego Human Research Protections Program. Ten healthy volunteers (6 male and 4 female), aged between 18 and 31 with an average age of 21, were recruited from the UC San Diego to participate in this study. This sample size fits a pilot study size (*14*). We sourced participants from different laboratories and organizations at UC San Diego where heterogeneous participants congregate. We did not rely on the same source to recruit new participants. These steps ensured a heterogeneous target pool of candidates of different ages and demographics. The ethnicity information of the participants was not collected at the time of the study. Informed consent was obtained from all participants. The participants had no visible skin cuts or infections in the application area. The participants were blinded for the input of stimulation. Inclusion criteria comprised healthy individuals between 18 and 40 years old. The age range of 18 to 40 was selected because of the lower likelihood of chronic diseases in this age group. Exclusion criteria included pregnancy, absence of skin injuries on or near the stimulation sites, rubber or elastomer allergies, highly sensitive skin, presence of pacemakers or other electrical or metal implants in the body, epilepsy or heart conditions, self-reported cancer or neurodegenerative diseases, and allergic reactions to topical moisturizers. We

evaluated the safety of our electrodes during stimulation using thermal infrared imaging to detect any joule heating effects (fig. S31). In addition, we measured the source voltage required to stimulate currents on the finger and the forearm in contrast to recent reports (fig. S32). After assessing safety protocols, our 10 human participants were subjected to experiments with the haptic device on the ventral forearm. Biphasic current stimulation is advisable to minimize pain perception and avoid half-cell reactions (*46*). Quantifying pain thresholds allowed us to know whether a participant would feel uncomfortable for succeeding tasks.

Electrical stimulation parameters

Before placing the electrode on the skin, we wanted to ensure that skin condition was as similar as possible between different participants because it has a strong influence on the variables and thus affects the sensation and comfort of stimulation. To remove the insulating layer of the stratum corneum that bears a high impedance of 100 kilohms, the skin was scraped gently with 3M Red Dot Trace Prep and with a 70% alcohol prep pad (*11*). In addition, given that the conductive path through the skin is not uniform at the microscopic level because of minute epithelial breaks, we used Q tips to minimally wet the surface with Milli-Q water before placing the electrode (*20*, *47*).

Stimulation was performed with constant current. Constant current is usually used because sweat can build up (*20*, *48*). A symmetric, biphasic, square waveform with 50% duty cycle was used. The square waveform is preferred because of its ease of implementation and interpretation in electrotactile feedback applications. In addition, the square waveform resulted in a faster depolarization of the nerve's axon, which promotes effective stimulation (*44*). A continuous biphasic waveform was used because it can prevent skin irritation caused by the transfer of ions within axon membranes, provide a wider range of stimulation parameters, and more effectively elicit diverse tactile sensations in lower currents. It also generates a better spread of current compared with monophasic stimulation (*49*, *50*). Modulation of one or more parameters, such as amplitude or frequency, can render different sensations. In general, the pulse width and amplitude may modulate the perceived intensity, whereas the frequency may modulate the perceived sensation (*51*, *52*). For the evaluation of elicited sensations, the frequency below 100 Hz was considered because earlier studies found that low frequency was the most useful range for sensory communication (*53*). The sensation elicited at 1 and 10 Hz represented a lower frequency, the sensation elicited at 50 Hz represented a mid frequency, and the sensation elicited at 100 Hz represented a higher frequency. The stimulus amplitudes were standardized across participants by using 1T, 2T, and 3T of each participant. The stimulation was applied via the surface electrode to either the forearm skin or the forehead. A commercial waveform generator and amplifier (BioPac STMISOLA) (fig. S34) were used to generate the studied stimuli. The electrode placement and stimulation setup are illustrated in figs. S33 and S34.

Measurement of pain threshold

One pair of electrodes was applied to the stimulation site. Participants rated the sensation of pain on a scale of 1 (not painful at all) to 5 (uncomfortably painful). A scale of 1 to 5 for pain detection was used because there is no uniform definition of pain (*20*). We stimulated the user's skin using 10 μA and increased the current amplitude in increments of 10 μA every 2 s until 250 μA had been reached or until the participant reported an uncomfortably painful sensation (5 on the scale). The frequency was set to 1 Hz. This process was repeated three times, with a 2-min break between each trial. We set an a priori exclusion criterion that any participant who reported an uncomfortably painful (5 on the scale) sensation in the stimulation range of 10 to 50 μA would be excluded from participating in the remainder of the experiment; no participants did so.

Measurement of detection threshold

We measured the detection threshold using a 2AFC detection task. Two pairs of electrodes were applied to the stimulation site (either the forehead or forearm). In each trial, only one of the two electrodes was stimulated, and participants were asked on which site they thought they had been stimulated (even if they were unsure, they were required to guess). There were a total of 128 trials per participant: eight trials for each combination of current (eight levels: 6, 8, 10, 12, 14, 16, 18, and 20 μA) and stimulation site (two levels) at a frequency of 1 Hz. The order of trials was randomized within each participant. We chose 16 trials per current level because it conveniently allowed us to operationalize "above detection threshold" using both the classical psychophysical definition (the current at which accuracy exceeded 75%, specifically 13 of 16 trials correct) and the statistical definition (the current at which accuracy was significantly higher than chance on a binomial test, also 13 of 16 trials correct).

Measurement of spatial acuity

We measured the spatial acuity (two-point discrimination) of the electrotactile current using a 2AFC discrimination task. Two electrode pairs were placed on the ventral side of the forearm, one near the medial epicondyle and the other near the wrist. The center-to-center distance between the inner electrode of the electrode pairs systematically varied from 2 to 10 cm in increments of 2 cm. Stimulation current was set to twice the participant's detection threshold at a frequency of 1 Hz. In each trial, stimulation was delivered to either one or both electrode pairs, and participants were asked whether they thought they had been stimulated in one versus two places (even if they were unsure, they were required to guess). There were a total of 30 trials per participant: three trials for each level of distance (five levels: 2, 4, 6, 8, and 10 cm) and stimulation type (two levels: one versus both positions stimulated). There were five blocks of six trials each: one block for each level of stimulus distance. The order of blocks was randomized within each participant, and the order of trials was randomized within each block.

The perceptual quality of sensation evaluation

We measured the perceptual quality of stimulation using a self-report questionnaire. One pair of electrodes was placed on the midpoint of the participant's forearm. We systematically varied the stimulation current and frequency to test perception under a wide range of stimulation parameters as follows: 1T, 1 Hz; 1T, 10 Hz; 2T, 1 Hz; 2T, 10 Hz; 3T, 1 Hz; 3T, 50 Hz; and 3T detection threshold, 100 Hz.

There were a total of 21 trials per participant: three trials for each combination of stimulation parameters (seven levels; see above). The order of presentation was randomized within each participant. In each trial, participants were asked to answer four questions regarding the sensation they felt, the comfort and intensity of stimulation, and the location of the sensation. The questions are described in detail in the Supplementary Materials in the section "Evaluation of the perceptual quality of sensation."

Contrast discrimination

We measured sensitivity to differences in current strength using a 2AFC task. Two pairs of stimulating electrodes were placed on the forearm by applying the detection limit current of the participants. On each trial, a different amount of current was delivered to each

electrode. One electrode was set to the participant's detection threshold, and the other was set to one of five different current amplitudes (1, 2, 3, 4, or 5 μA higher than the participant's detection threshold). For example, if a participant had a detection threshold of 10 μA, in a given trial, one electrode would deliver 10 μA and the other would deliver either 11, 12, 13, 14, or 15 μA. In each trial, the electrode delivering the higher current was varied, and the participant was asked at which electrode they thought the sensation was more intense (even if they were unsure, they were required to guess). There were a total of 40 trials per participant: four for each combination of current (five levels) and location of higher current (two levels). The order of trials was randomized within participants.

Statistical analysis

In general, psychophysical experimental data were fit using mixed effect regression frameworks and generalized linear mixed models (GLMMs; either linear or binomial with logit link function, depending on the dependent variable), which are more powerful than alternatives like *t* tests on *d′* because GLMMs account for participants' performance in each trial rather than averaging across trials (*54*). For each experiment, we fit a GLMM with trial outcome as the dependent variable and participant as random effect; the independent variables were experiment dependent and are described in detail in each subsection below. GLMMs were fit using the lme4 package in R (*55*), and participant performance at specific levels of the independent variables was assessed using estimated marginal means, calculated using the estimated marginal means (emmeans) package in R (*56*). All *P* values reported in the manuscript are from Wald tests on either regression parameters or estimated marginal means (*57*).

Measurement of detection threshold

To quantify the effect of stimulation current on detection accuracy, data from the 2AFC detection task were fit using a logistic mixed effect regression (GLMM) with fixed effect of log stimulation current, random effect of participant, and dependent variable of trial outcome (correct/incorrect). Overall, participants were significantly more accurate when stimulation current was higher [GLMM fixed effect $\beta_{\log(I)} = 1.79$, $SE_{\log(\beta I)} = 0.25$, Wald $Z = 7.20$, $P < 0.001$]; on average, each 60% increase in stimulation current doubled the odds of detecting the stimulus. Nevertheless, even at the lowest stimulation current used in the study, participants' performance was much higher than chance [estimated marginal mean, $P(\text{correct})_{I = 6\ \text{mA}} = 0.84$; 95% confidence interval (CI) (0.66, 0.94)] and higher than the 75% accuracy criterion classically used to define the sensory detection threshold (*58*). We conducted Bonferroni-corrected Wald *Z* tests ($\alpha = 0.006$) of the estimated marginal means at all current levels, and participants' accuracy was significantly greater than chance at all eight current levels (all $P < 0.001$).

Measurement of spatial acuity

To quantify participants' two-point discrimination, data from the 2AFC two-point discrimination task were fit using a logistic mixed effect regression (GLMM) with fixed effect of electrode distance, random effect of participant, and dependent variable of trial outcome (correct/incorrect). Overall, two-point discrimination was significantly higher than chance [GLMM estimated marginal mean, $P(\text{correct}) = 0.96$, SE = 0.01, Wald $Z = 10.68$, $P < 0.001$]. There was not a significant relationship between electrode distance and two-point discrimination (GLMM fixed effect $\beta_d = 0.07$, $SE_{\beta d} = 0.11$, Wald $Z = 0.62$, $P = 0.53$). This null effect of electrode distance is plausibly a ceiling effect because of the physical constraint of electrode spacing: Even at the smallest distance possible for our setup (2 cm), accuracy was 93% [estimated marginal mean; 95% CI (0.88, 0.98)], and for 7 of the 10 participants, accuracy was 100%. Note that the GLMM model yielded a singular fit with near-zero variance in the random effect (likely because so many participants had near-perfect performance); so, to verify that this did not influence our interpretation, we reran the analysis as a logistic regression with an independent variable of separation distance and a dependent variable of trial outcome (such as dropping the random effect from the model). Doing so did not change the result; the coefficients were the same as reported above (when rounded to two significant digits).

To quantify two-point discrimination at specific distances (as reported in the main manuscript), we conducted Bonferroni-corrected Wald *Z* tests ($\alpha = 0.01$) of the estimated marginal means. Participants' accuracy was significantly greater than chance at all five distances (all $P < 0.001$).

The perceptual quality of sensation evaluation

Qualitative sensation was evaluated across all combinations of stimulation frequency and current in the study. Participants predominantly reported the sensation of either pressure or vibration; in fewer than 5% of trials, a different sensation was reported (itchiness or warmth). We classified these trials as outliers and removed them from further analyses. To quantify the relationship among stimulation frequency, stimulation current, and reported sensation (vibration versus pressure), data were fit using a logistic mixed effect regression (GLMM) with fixed effects of (log-transformed) stimulation frequency, (log-transformed) stimulation current, and their interaction; random effect of participant; and dependent variable of reported sensation (vibration versus pressure). Overall, participants were significantly more likely to experience vibration when stimulation frequency was higher [GLMM fixed effect $\beta_{\log(f)} = 1.31$, $SE_{\beta\log(f)} = 0.33$, Wald $Z = 3.96$, $P < 0.001$]. On average, increasing the stimulation frequency by 70% doubled the odds of experiencing vibration (versus pressure), and the model predicts that the crossover point at which participants first begin to report vibration more often than pressure is ~6 Hz. In contrast to the effect of stimulation frequency, stimulation current did not significantly influence the type of sensation reported by participants [GLMM fixed effect $\beta_{\log(I) \times \log(f)}$ and $\beta_{\log(I)}$ terms; both $P > 0.2$].

The intensity rating for changes in stimulation current was assessed. Whereas changes in stimulation frequency produced qualitatively different sensations (pressure versus vibration), changes in stimulation current seemed to produce quantitatively different sensations (more versus less intense). To quantify this observation, data were fit using a linear mixed effect regression (LMM) with fixed effects of log stimulation frequency, log stimulation current, and their interaction; random effect of participant; and dependent variable of reported intensity (1 to 5 scale). Overall, the sensation produced by stronger currents was rated as significantly more intense [LMM fixed effect $\beta_{\log(I)} = 0.36$, $SE_{\beta\log(I)} = 0.05$, $t(176.01) = 3.18$, $P = 0.002$]; on average, doubling the stimulation current increased the intensity rating by approximately 0.25 (on the 1 to 5 scale).

Next, we assessed the amount of discomfort during stimulations. All sensations were reported to be between very comfortable and neutral except for a single trial for a single participant (who rated 10-Hz stimulation at detection threshold as uncomfortable).

In addition, we assessed the localization of the perceived stimulation. Almost all sensations (93%) were experienced as localized rather than radiating (5%) or referred (1%). To quantify the relationship between stimulation frequency, stimulation current, and reported

location, data were fit using a logistic mixed effect regression (GLMM) with fixed effects of log stimulation frequency, log stimulation current, and their interaction; random effect of participant; and dependent variable of reported location (localized/not localized, dummy coded as 1/0). The probability of experiencing a sensation as localized did not significantly depend on frequency or current [GLMM fixed effect $\beta_{\log(I) \times \log(f)}$ and $\beta_{\log(I)}$ terms; both $P > 0.05$]. Overall, participants experienced the sensations as localized far more often than would be predicted by chance [GLMM estimated marginal mean, $P(\text{localized}) > 0.99$, $\text{SE} = 0.009$, Wald $Z = 2.78$, $P = 0.005$].

Contrast discrimination

To quantify participants' ability to discriminate between two different stimulation currents, data from the 2AFC discrimination task were fit using a logistic mixed effect regression (GLMM) with fixed effect of difference in (log-scaled) stimulation current, random effect of participant, and dependent variable of trial outcome (correct/incorrect). Overall, participants were significantly more accurate when the two stimulation currents were more different [GLMM fixed effect $\beta_{\Delta\log(I)} = 5.92$, $\text{SE}_{\Delta\log(I)} = 1.00$, Wald $Z = 5.94$, $P < 0.001$]; on average, each 13% increase in the difference between stimulation currents doubled the odds of detecting the difference. Furthermore, the smallest difference for which $P(\text{correct}) > 0.75$ (specifically, the psychophysical threshold for discrimination) was 1.33 times the detection threshold [as estimated by GLMM estimated marginal mean, $P(\text{correct} \mid \Delta\log(I) = 1.33) = 0.75$].

Commercial dual electrodes

For the comparison study, we used Ag/AgCl electrodes (EL507, BIOPAC Systems Inc.) with electrode gel (Spectra 360, BIOPAC Systems Inc.).

Supplementary Materials

This PDF file includes:

Methods
Figs. S1 to S43
Tables S1 to S3
References (*64*–*101*)

Other Supplementary Material for this manuscript includes the following:

MDAR Reproducibility Checklist

REFERENCES AND NOTES

1. M. Kitagawa, D. Dokko, A. M. Okamura, D. D. Yuh, Effect of sensory substitution on suture-manipulation forces for robotic surgical systems. *J. Thorac. Cardiovasc. Surg.* **129**, 151–158 (2005).
2. H. J. B. Witteveen, E. A. Droog, J. S. Rietman, P. H. Veltink, Vibro- and electrotactile user feedback on hand opening for myoelectric forearm prostheses. *IEEE Trans. Biomed. Eng.* **59**, 2219–2226 (2012).
3. D. S. Pamungkas, K. Ward, Electro-tactile feedback system to enhance virtual reality experience. *Int. J. Comput. Theory* **8**, 465–470 (2016).
4. C. V. Keef, L. V. Kayser, S. Tronboll, C. W. Carpenter, N. B. Root, M. Finn, T. F. O'Connor, S. N. Abuhamdieh, D. M. Davies, R. Runser, Y. S. Meng, V. S. Ramachandran, D. J. Lipomi, Virtual texture generated using elastomeric conductive block copolymer in a wireless multimodal haptic glove. *Adv. Intell. Syst.* **2**, 2000018 (2020).
5. V. Bucciarelli, N. Gozzi, N. Katic, G. Aiello, M. Razzoli, G. Valle, S. Raspopovic, Multiparametric non-linear TENS modulation to integrate intuitive sensory feedback. *J. Neural Eng.* **20**, 036026 (2023).
6. W. Lin, D. Zhang, W. W. Lee, X. Li, Y. Hong, Q. Pan, R. Zhang, G. Peng, H. Z. Tan, Z. Zhang, L. Wei, Z. Yang, Super-resolution wearable electrotactile rendering system. *Sci. Adv.* **8**, eabp8738 (2022).
7. Y. H. Jung, J. H. Kim, J. A. Rogers, Skin-integrated vibrohaptic interfaces for virtual and augmented reality. *Adv. Funct. Mater.* **31**, 2008805 (2021).
8. A. Akhtar, J. Sombeck, B. Boyce, T. Bretl, Controlling sensation intensity for electrotactile stimulation in human-machine interfaces. *Sci. Robot.* **3**, eaap9770 (2018).
9. L. P. Paredes, S. Dosen, F. Rattay, B. Graimann, D. Farina, The impact of the stimulation frequency on closed-loop control with electrotactile feedback. *J. Neuroeng. Rehabil.* **12**, 35 (2015).
10. B. Geng, J. Dong, W. Jensen, S. Dosen, D. Farina, E. N. Kamavuako, Psychophysical evaluation of subdermal electrical stimulation in relation to prosthesis sensory feedback. *IEEE Trans. Neural Syst. Rehabil. Eng.* **26**, 709–715 (2018).
11. A. Mazzotta, M. Carlotti, V. Mattoli, Conformable on-skin devices for thermo-electro-tactile stimulation: Materials, design, and fabrication. *Mater. Adv.* **2**, 1787–1820 (2021).
12. X. Yu, Z. Xie, Y. Yu, J. Lee, A. Vazquez-Guardado, H. Luan, J. Ruban, X. Ning, A. Akhtar, D. Li, B. Ji, Y. Liu, R. Sun, J. Cao, Q. Huo, Y. Zhong, C. M. Lee, S. Y. Kim, P. Gutruf, C. Zhang, Y. Xue, Q. Guo, A. Chempakasseril, P. Tian, W. Lu, J. Y. Jeong, Y. J. Yu, J. Cornman, C. S. Tan, B. H. Kim, K. H. Lee, X. Feng, Y. Huang, J. A. Rogers, Skin-integrated wireless haptic interfaces for virtual and augmented reality. *Nature* **575**, 473–479 (2019).
13. C. Pacchierotti, S. Sinclair, M. Solazzi, A. Frisoli, V. Hayward, D. Prattichizzo, Wearable haptic systems for the fingertip and the hand: Taxonomy, review, and perspectives. *IEEE Trans. Haptics* **10**, 580–600 (2017).
14. P. Kourtesis, F. Argelaguet, S. Vizcay, M. Marchal, C. Pacchierotti, Electrotactile feedback applications for hand and arm interactions: A systematic review, meta-analysis, and future directions. *IEEE Trans. Haptics* **15**, 479–496 (2022).
15. Y. Luo, M. R. Abidian, J.-H. Ahn, D. Akinwande, A. M. Andrews, M. Antonietti, Z. Bao, M. Berggren, C. A. Berkey, C. J. Bettinger, J. Chen, P. Chen, W. Cheng, X. Cheng, S.-J. Choi, A. Chortos, C. Dagdeviren, R. H. Dauskardt, C. Di, M. D. Dickey, X. Duan, A. Facchetti, Z. Fan, Y. Fang, J. Feng, X. Feng, H. Gao, W. Gao, X. Gong, C. F. Guo, X. Guo, M. C. Hartel, Z. He, J. S. Ho, Y. Hu, Q. Huang, Y. Huang, F. Huo, M. M. Hussain, A. Javey, U. Jeong, C. Jiang, X. Jiang, J. Kang, D. Karnaushenko, A. Khademhosseini, D.-H. Kim, I.-D. Kim, D. Kireev, L. Kong, C. Lee, N.-E. Lee, P. S. Lee, T.-W. Lee, F. Li, J. Li, C. Liang, C. T. Lim, Y. Lin, D. J. Lipomi, J. Liu, K. Liu, N. Liu, R. Liu, Y. Liu, Y. Liu, Z. Liu, Z. Liu, X. J. Loh, N. Lu, Z. Lv, S. Magdassi, G. G. Malliaras, N. Matsuhisa, A. Nathan, S. Niu, J. Pan, C. Pang, Q. Pei, H. Peng, D. Qi, H. Ren, J. A. Rogers, A. Rowe, O. G. Schmidt, T. Sekitani, D.-G. Seo, G. Shen, X. Sheng, Q. Shi, T. Someya, Y. Song, E. Stavrinidou, M. Su, X. Sun, K. Takei, X.-M. Tao, B. C. K. Tee, A. V.-Y. Thean, T. Q. Trung, C. Wan, H. Wang, J. Wang, M. Wang, S. Wang, T. Wang, Z. L. Wang, P. S. Weiss, H. Wen, S. Xu, T. Xu, H. Yan, X. Yan, H. Yang, L. Yang, S. Yang, L. Yin, C. Yu, G. Yu, J. Yu, S.-H. Yu, X. Yu, E. Zamburg, H. Zhang, X. Zhang, X. Zhang, X. Zhang, Y. Zhang, Y. Zhang, S. Zhao, X. Zhao, Y. Zheng, Y.-Q. Zheng, Z. Zheng, T. Zhou, B. Zhu, M. Zhu, R. Zhu, Y. Zhu, Y. Zhu, G. Zou, X. Chen, Technology roadmap for flexible sensors. *ACS Nano* **17**, 5211–5295 (2023).
16. E. L. Graczyk, M. A. Schiefer, H. P. Saal, B. P. Delhaye, S. J. Bensmaia, D. J. Tyler, The neural basis of perceived intensity in natural and artificial touch. *Sci. Transl. Med.* **8**, 362ra142 (2016).
17. B. Stephens-Fripp, R. Mutlu, G. Alici, A comparison between separated electrodes and concentric electrodes for electrotactile stimulation. *IEEE Trans. Med. Robot. Bionics* **3**, 241–252 (2021).
18. R. Blau, A. X. Chen, B. Polat, L. L. Becerra, R. Runser, B. Zamanimeymian, K. Choudhary, D. J. Lipomi, Intrinsically stretchable block copolymer based on PEDOT:PSS for improved performance in bioelectronic applications. *ACS Appl. Mater. Interfaces* **14**, 4823–4835 (2022).
19. L. V. Kayser, D. J. Lipomi, Stretchable conductive polymers and composites based on PEDOT and PEDOT:PSS. *Adv. Mater.* **31**, e1806133 (2019).
20. K. A. Kaczmarek, J. G. Webster, P. Bach-y-Rita, W. J. Tompkins, Electrotactile and vibrotactile displays for sensory substitution systems. *IEEE Trans. Biomed. Eng.* **38**, 1–16 (1991).
21. C. Lim, Y. J. Hong, J. Jung, Y. Shin, S. H. Sunwoo, S. Baik, O. K. Park, S. H. Choi, T. Hyeon, J. H. Kim, S. Lee, D. H. Kim, Tissue-like skin-device interface for wearable bioelectronics by using ultrasoft, mass-permeable, and low-impedance hydrogels. *Sci. Adv.* **7**, eabd3716 (2021).
22. G. Corniani, H. P. Saal, Tactile innervation densities across the whole body. *J. Neurophysiol.* **124**, 1229–1240 (2020).
23. W. Wang, Y. Jiang, D. Zhong, Z. Zhang, S. Choudhury, J. C. Lai, H. Gong, S. Niu, X. Yan, Y. Zheng, C. C. Shih, R. Ning, Q. Lin, D. Li, Y. H. Kim, J. Kim, Y. X. Wang, C. Zhao, C. Xu, X. Ji, Y. Nishio, H. Lyu, J. B. H. Tok, Z. Bao, Neuromorphic sensorimotor loop embodied by monolithically integrated, low-voltage, soft e-skin. *Science* **380**, 735–742 (2023).
24. E. Losanno, M. Mender, C. Chestek, S. Shokur, S. Micera, Neurotechnologies to restore hand functions. *Nat. Rev. Bioeng.* **1**, 390–407 (2023).
25. R. K. Ray, P. Patel, M. Manivannan, Reduction of electrotactile perception threshold using subthreshold vibrotactile stimuli. *Displays* **69**, 102056 (2021).
26. G. Alon, G. Kantor, H. S. Ho, Effects of electrode size on basic excitatory responses and on selected stimulus parameters. *J. Orthop. Sports Phys. Ther.* **20**, 29–35 (1994).
27. H. Yuk, B. Lu, X. Zhao, Hydrogel bioelectronics. *Chem. Soc. Rev.* **48**, 1642–1667 (2019).
28. K. Tybrandt, I. V. Zozoulenko, M. Berggren, Chemical potential-electric double layer coupling in conjugated polymer-polyelectrolyte blends. *Sci. Adv.* **3**, eaao3659 (2017).
29. B. D. Paulsen, K. Tybrandt, E. Stavrinidou, J. Rivnay, Organic mixed ionic–electronic conductors. *Nat. Mater.* **19**, 13–26 (2020).

30. A. V. Volkov, K. Wijeratne, E. Mitraka, U. Ail, D. Zhao, K. Tybrandt, J. W. Andreasen, M. Berggren, X. Crispin, I. V. Zozoulenko, Understanding the capacitance of PEDOT:PSS. *Adv. Funct. Mater.* **27**, 1700329 (2017).
31. R. Vatsyayan, S. A. Dayeh, A universal model of electrochemical safety limits in vivo for electrophysiological stimulation. *Front. Neurosci.* **16**, 972252 (2022).
32. D.-H. Kim, N. Lu, R. Ma, Y.-S. Kim, R.-H. Kim, S. Wang, J. Wu, S. M. Won, H. Tao, A. Islam, K. J. Yu, T.-I. Kim, R. Chowdhury, M. Ying, L. Xu, M. Li, H.-J. Chung, H. Keum, M. Mccormick, P. Liu, Y.-W. Zhang, F. G. Omenetto, Y. Huang, T. Coleman, J. A. Rogers, Epidermal electronics. *Science* **333**, 838–843 (2011).
33. C. Ruisheng Guo, Y. Yu, Z. Xie, X. Liu, X. Zhou, Y. Gao, Z. Liu, F. Zhou, Y. Yang, Z. Zheng, R. Guo, F. Zhou, Y. Yu, Z. Xie, X. Liu, X. Zhou, Y. Gao, Z. Liu, Z. J. Zheng, Y. Yang, Matrix-assisted catalytic printing for the fabrication of multiscale, flexible, foldable, and stretchable metal conductors. *Adv. Mater.* **25**, 3343–3350 (2013).
34. H. Song, G. Luo, Z. Ji, R. Bo, Z. Xue, D. Yan, F. Zhang, K. Bai, J. Liu, X. Cheng, W. Pang, Z. Shen, Y. Zhang, Highly-integrated, miniaturized, stretchable electronic systems based on stacked multilayer network materials. *Sci. Adv.* **8**, eabm3785 (2022).
35. M. Moroni, M. R. Servin-Vences, R. Fleischer, O. Sánchez-Carranza, G. R. Lewin, Voltage gating of mechanosensitive PIEZO channels. *Nat. Commun.* **9**, 1096 (2018).
36. D. R. McNeal, Analysis of a model for excitation of myelinated nerve. *IEEE Trans. Biomed. Eng.* **4**, 329–337 (1976).
37. S. G. Lechner, G. R. Lewin, Hairy sensation. *Physiology* **28**, 142–150 (2013).
38. Å. B. Vallbo, Sensations evoked from the glabrous skin of the human hand by electrical stimulation of unitary mechanosensitive afferents. *Brain Res.* **215**, 359–363 (1981).
39. D. Purves, Cutaneous and subcutaneous somatic sensory receptors, in *Neuroscience*, D. Purves, Ed. (Sinauer Associates, ed. 3, 2004), pp. 189–208.
40. S. P. McKee, L. Welch, Sequential recruitment in the discrimination of velocity. *J. Opt. Soc. Am. A* **2**, 243–251 (1985).
41. A. Ikoma, H. Handwerker, Y. Miyachi, M. Schmelz, Electrically evoked itch in humans. *Pain* **113**, 148–154 (2005).
42. Y. Huang, K. Yao, J. Li, D. Li, H. Jia, Y. Liu, C. K. Yiu, W. Park, X. Yu, Recent advances in multi-mode haptic feedback technologies towards wearable interfaces. *Mater. Today Phys.* **22**, 100602 (2022).
43. I. Birznieks, S. McIntyre, H. M. Nilsson, S. S. Nagi, V. G. Macefield, D. A. Mahns, R. M. Vickery, Tactile sensory channels over-ruled by frequency decoding system that utilizes spike pattern regardless of receptor type. *eLife* **8**, e46510 (2019).
44. C. Pasluosta, P. Kiele, T. Stieglitz, Paradigms for restoration of somatosensory feedback via stimulation of the peripheral nervous system. *Clin. Neurophysiol.* **129**, 851–862 (2018).
45. M. Solomonow, J. Lyman, A. Freedy, Electrotactile two-point discrimination as a function of frequency, body site, laterality, and stimulation codes. *Ann. Biomed. Eng.* **5**, 47–60 (1977).
46. S. Mottaghi, N. Afshari, O. Buchholz, S. Liebana, U. G. Hofmann, Modular current stimulation system for pre-clinical studies. *Front. Neurosci.* **14**, 408 (2020).
47. A. Y. J. Szeto, F. A. Saunders, Electrocutaneous stimulation for sensory communication in rehabilitation engineering. *IEEE Trans. Biomed. Eng.* **BME-29**, 300–308 (1982).
48. J. L. Mason, N. Mackay, Pain sensations associated with electrocutaneous stimulation. *IEEE Trans. Biomed. Eng.* **BME-23**, 405–409 (1976).
49. F. A. Lenz, M. Seike, R. T. Richardson, Y. C. Lin, F. H. Baker, I. Khoja, C. J. Jaeger, R. H. Gracely, Thermal and pain sensations evoked by microstimulation in the area of human ventrocaudal nucleus. *J. Neurophysiol.* **70**, 200–212 (1993).
50. D. S. Pamungkas, W. Caesarendra, Overview electrotactile feedback for enhancing human computer interface. *J. Phys. Conf. Ser.* **1007**, 012001 (2018).
51. D. J. Djozic, D. Bojanic, G. Krajoski, N. Popov, V. Ilic, Psychophysical characteristics of electrotactile stimulation: The impact of changes in stimulation pulse width and frequency on human perception, in *2015 IEEE 15th International Conference on Bioinformatics and Bioengineering (BIBE)* (IEEE, 2015), pp. 1–5.
52. K. A. Kaczmarek, M. E. Tyler, A. J. Brisben, K. O. Johnson, The afferent neural response to electrotactile stimuli: Preliminary results. *IEEE Trans. Rehabil. Eng.* **8**, 268–270 (2000).
53. A. Y. J. Szeto, J. Lyman, R. E. Prior, Electrocutaneous pulse rate and pulse width psychometric functions for sensory communications. *Hum. Factors* **21**, 241–249 (1979).
54. A. Moscatelli, M. Mezzetti, F. Lacquaniti, Modeling psychophysical data at the population-level: The generalized linear mixed model. *J. Vis.* **12**, 26 (2012).
55. D. Bates, M. Mächler, B. M. Bolker, S. C. Walker, Fitting linear mixed-effects models using lme4. *J. Stat. Softw.* **67**, 1–48 (2015).
56. S. R. Searle, F. M. Speed, G. A. Milliken, R. Searle, Population marginal means in the linear model: An alternative to least squares means. *Am. Stat.* **34**, 216–221 (1980).
57. A. Wald, Tests of statistical hypotheses concerning several parameters when the number of observations is large. *Trans. Am. Math. Soc.* **54**, 426–482 (1943).
58. S. P. Mckee, S. A. Klein, D. Y. Teller, Statistical properties of forced-choice psychometric functions: Implications of probit analysis. *Percept. Psychophys.* **37**, 286–298 (1985).
59. N. Kim, S. Lienemann, I. Petsagkourakis, D. Alemu Mengistie, S. Kee, T. Ederth, V. Gueskine, P. Leclère, R. Lazzaroni, X. Crispin, K. Tybrandt, Elastic conducting polymer composites in thermoelectric modules. *Nat. Commun.* **11**, 1424 (2020).
60. Y. Li, X. Li, S. Zhang, L. Liu, N. Hamad, S. R. Bobbara, D. Pasini, F. Cicoira, Autonomic self-healing of PEDOT:PSS achieved via polyethylene glycol addition. *Adv. Funct. Mater.* **30**, 2002853 (2020).
61. Y. Jiang, Z. Zhang, Y. X. Wang, D. Li, C. T. Coen, E. Hwaun, G. Chen, H. C. Wu, D. Zhong, S. Niu, W. Wang, A. Saberi, J. C. Lai, Y. Wu, Y. Wang, A. A. Trotsyuk, K. Y. Loh, C. C. Shih, W. Xu, K. Liang, K. Zhang, Y. Bai, G. Gurusankar, W. Hu, W. Jia, Z. Cheng, R. H. Dauskardt, G. C. Gurtner, J. B. H. Tok, K. Deisseroth, I. Soltesz, Z. Bao, Topological supramolecular network enabled high-conductivity, stretchable organic bioelectronics. *Science* **375**, 1411–1417 (2022).
62. C. Xu, S. Yang, P. Li, H. Wang, H. Li, Z. Liu, Wet-spun PEDOT:PSS/CNT composite fibers for wearable thermoelectric energy harvesting. *Compos. Commun.* **32**, 101179 (2022).
63. A. W. Roe, R. M. Friedman, L. M. Chen, Multiple representation in primate SI: A view from a window on the brain, in *Handbook of Neurochemistry and Molecular Neurobiology: Sensory Neurochemistry*, A. Lajtha, D. A. Johnson, Eds. (Springer, 2007), pp. 1–16.
64. W. Humphrey, A. Dalke, K. Schulten, VMD: Visual molecular dynamics. *J. Mol. Graph.* **14**, 33–38 (1996).
65. S. L. Mayo, B. D. Olafson, W. A. Goddard, DREIDING: A generic force field for molecular simulations. *J. Phys. Chem.* **94**, 8897–8909 (1990).
66. A. P. Thompson, H. M. Aktulga, R. Berger, D. S. Bolintineanu, W. M. Brown, P. S. Crozier, P. J. in 't Veld, A. Kohlmeyer, S. G. Moore, T. D. Nguyen, R. Shan, M. J. Stevens, J. Tranchida, C. Trott, S. J. Plimpton, LAMMPS - a flexible simulation tool for particle-based materials modeling at the atomic, meso, and continuum scales. *Comput. Phys. Commun.* **271**, 108171 (2022).
67. T. Shire, K. J. Hanley, K. Stratford, DEM simulations of polydisperse media: Efficient contact detection applied to investigate the quasi-static limit. *Comput. Part. Mech.* **8**, 653–663 (2021).
68. P. J. in 't Veld, S. J. Plimpton, G. S. Grest, Accurate and efficient methods for modeling colloidal mixtures in an explicit solvent using molecular dynamics. *Comput. Phys. Commun.* **179**, 320–329 (2008).
69. A. Kausar, Fabrication and characteristics of poly(benzimidazole/fluoro/ether/siloxane/amide)/sulfonated polystyrene/silica nanoparticle-based proton exchange membranes doped with phosphoric acid. *Int. J. Polym. Mater. Polym. Biomater.* **64**, 184–191 (2014).
70. B. T. N. C. Andrade, A. C. D. S. Bezerra, C. R. Calado, Adding value to polystyrene waste by chemically transforming it into sulfonated polystyrene. *Matéria (Rio de Janeiro)* **24**, e12417 (2019).
71. B. W. Chieng, N. A. Ibrahim, W. M. Z. W. Yunus, M. Z. Hussein, Poly(lactic acid)/poly(ethylene glycol) polymer nanocomposites: Effects of graphene nanoplatelets. *Polymers* **6**, 93–104 (2014).
72. N. S. Vrandečić, M. Erceg, M. Jakić, I. Klarić, Kinetic analysis of thermal degradation of poly(ethylene glycol) and poly(ethylene oxide)s of different molecular weight. *Thermochim. Acta* **498**, 71–80 (2010).
73. W. W. Chiu, J. Travaš-Sejdić, R. P. Cooney, G. A. Bowmaker, Studies of dopant effects in poly(3,4-ethylenedi-oxythiophene) using Raman spectroscopy. *J. Raman Spectrosc.* **37**, 1354–1361 (2006).
74. S. Nešpůrek, P. Kuberský, R. Polanský, M. Trchová, J. Šebera, V. Sychrovský, Raman spectroscopy and DFT calculations of PEDOT:PSS in a dipolar field. *Phys. Chem. Chem. Phys.* **24**, 541–550 (2021).
75. R. Wang, Y. Wang, C. Wu, T. Zhai, J. Yang, B. Sun, S. Duhm, N. Koch, Direct observation of conductive polymer induced inversion layer in n-Si and correlation to solar cell performance. *Adv. Funct. Mater.* **30**, 1903440 (2020).
76. S. Ne Perrot, F. Pawula, S. Pechev, G. Hadziioannou, G. Fleury, PEDOT:Tos electronic and thermoelectric properties: Lessons from two polymerization processes. *J. Mater. Chem. C* **9**, 7417–7425 (2021).
77. C. V. Amanchukwu, M. Gauthier, T. P. Batcho, C. Symister, Y. Shao-Horn, J. M. D'arcy, P. T. Hammond, Evaluation and stability of PEDOT polymer electrodes for Li–O_2 batteries. *J. Phys. Chem. Lett.* **7**, 3770–3775 (2016).
78. S. Bhatt, J. Pulpytel, M. Mirshahi, F. Arefi-Khonsari, Catalyst-free plasma-assisted copolymerization of poly(ε-caprolactone)-poly(ethylene glycol) for biomedical applications. *ACS Macro Lett.* **1**, 764–767 (2012).
79. L. H. Rong, X. Cheng, J. Ge, O. K. Krebs, J. R. Capadona, E. B. Caldona, R. C. Advincula, SI-PET-RAFT polymerization via electrodeposited macroinitiator thin films: Toward biomedical and sensing applications. *ACS Appl. Polym. Mater.* **4**, 6449–6457 (2022).
80. G. M. Veith, M. Doucet, R. L. Sacci, B. Vacaliuc, J. K. Baldwin, J. F. Browning, Determination of the solid electrolyte interphase structure grown on a silicon electrode using a fluoroethylene carbonate additive. *Sci. Rep.* **7**, 6326 (2017).
81. R. Bütikofer, P. D. Lawrence, Electrocutaneous nerve stimulation—I: Model and experiment. *IEEE Trans. Biomed. Eng.* **6**, 526–531 (1978).
82. T. Edmond, A. Laps, A. L. Case, N. O'Hara, J. M. Abzug, Normal ranges of upper extremity length, circumference, and rate of growth in the pediatric population. *Hand* **15**, 713–721 (2020).
83. G. Li, S. Wang, Y. Y. Duan, Towards gel-free electrodes: A systematic study of electrode-skin impedance. *Sens. Actuators B Chem.* **241**, 1244–1255 (2017).
84. I. J. Jossinet, A. Lackermeier, F. Risacher, Factors affecting electrode-gel-skin interface impedance in electrical impedance tomography. *Biol. Eng. Comput.* **34**, 397–408 (1996).

85. K. Geoffrey, H. Reeves, Barry Harrison, obtaining the specific contact resistance from transmission line model measurements. *IEEE Electron Device Lett.* **3**, 111–113 (1982).
86. Y. Park, C. K. Franz, H. Ryu, H. Luan, K. Y. Cotton, J. Uk Kim, T. S. Chung, S. Zhao, A. Vazquez-Guardado, D. Som Yang, K. Li, R. Avila, J. K. Phillips, M. J. Quezada, H. Jang, S. Soo Kwak, S. Min Won, K. Kwon, H. Jeong, A. J. Bandodkar, M. Han, H. Zhao, G. R. Osher, H. Wang, K. Lee, Y. Zhang, Y. Huang, J. D. Finan, J. A. Rogers, Three-dimensional, multifunctional neural interfaces for cortical spheroids and engineered assembloids. *Sci. Adv.* **7**, 9153–9170 (2021).
87. A. Wiranata, S. Maeda, Implementation of SYLGARD 184 for powder-based dielectric elastomer actuators. *SEATUC J. Sci. Eng.* **1**, 14–19 (2020).
88. M. Rahimi, F. Jiang, Y. Shen, Spatiotemporal identification of moving patterns on a fingertip-based electro-tactile display array. *TechRxiv* 1–10 (2020).
89. S. E. Root, C. W. Carpenter, L. V. Kayser, D. Rodriquez, D. M. Davies, S. Wang, S. T. M. Tan, Y. S. Meng, D. J. Lipomi, Ionotactile stimulation: Nonvolatile ionic gels for human-machine interfaces. *ACS Omega* **3**, 662–666 (2018).
90. H. Kajimoto, Electrotactile display with real-time impedance feedback using pulse width modulation. *IEEE Trans. Haptics* **5**, 184–188 (2012).
91. H. Kajimoto, N. Kawakami, S. Tachi, Electro-tactile display with tactile primary color approach, Graduate School of Information and Technology, University of Tokyo (2004).
92. S. Gabriel, R. W. Lau, C. Gabriel, The dielectric properties of biological tissues: II. Measurements in the frequency range 10 Hz to 20 GHz. *Phys. Med.* **41**, 2251–2269 (1996).
93. Y. E. Shuan, K. Zhu, P. Li, S. Xiaohong, Neural firing mechanism underlying two-electrode discrimination by 3D transcutaneous electrical nerve stimulation computational model. *J. Shanghai Jiao Tong Univ. (Sci.)* **24**, 716–722 (2019).
94. C. Koch, The Hodgkin and Huxley model of action potential generation, in *Biophysics of Computation*, C. Koch, Ed. (Oxford Univ. Press, 2004), pp. 139–174.
95. M. Franceschi, L. Seminara, S. Dosen, M. Strbac, M. Valle, D. Farina, A system for electrotactile feedback using electronic skin and flexible matrix electrodes: Experimental evaluation. *IEEE Trans. Haptics* **10**, 162–172 (2017).
96. B. Geng, K. Yoshida, L. Petrini, W. Jensen, Evaluation of sensation evoked by electrocutaneous stimulation on forearm in nondisabled subjects. *J. Rehabil. Res. Dev.* **49**, 297–308 (2012).
97. T. Tashiro, The perceptual properties of electrocutaneous stimulation: Sensory quality, subjective intensity, and intensity-duration relation. *Percept. Psychophys.* **30**, 579–586 (1981).
98. M. Perović, M. Stevanović, T. Jevtić, M. Štrbac, G. Bijelić, Č. Vučetić, L. Popović-Maneski, D. B. Popović, Electrical stimulation of the forearm: A method for transmitting sensory signals from the artificial hand to the brain. *J. Autom. Control* **21**, 13–18 (2013).
99. V. Yem, H. Kajimoto, Comparative evaluation of tactile sensation by electrical and mechanical stimulation. *IEEE Trans. Haptics* **10**, 130–134 (2017).
100. K. Choi, P. Kim, K. S. Kim, S. Kim, Mixed-modality stimulation to evoke two modalities simultaneously in one channel for electrocutaneous sensory feedback. *IEEE Trans. Neural Syst. Rehabil. Eng.* **25**, 2258–2269 (2017).
101. H. Kajimoto, N. Kawakami, S. Tachi, Psychophysical evaluation of receptor selectivity in electro-tactile display, in *Proceedings of the 13th International Symposium on Measurement and Control in Robotics (ISMCR)* (IEEE, 2003), pp. 83–86.

Acknowledgments: We thank J. Bae and L. Tang for their support with optical microscopy measurements, N. Boechler for helpful discussions, P. Rangamani and M. Quintana for their guidance with computational biophysics, and I. C. Tran for help with XPS analysis. Work was performed using instrumentation funded in part by the National Science Foundation Major Research Instrumentation Program under grant no. CHE-1338173. Elements of Figs. 3 (A and B) and 4C were illustrated by BioRender.com. **Funding:** This work was supported by the National Science Foundation Disability and Rehabilitation Engineering program under grant no. CBET-2223566. Aspects of the development of the conductive block copolymer were supported by Air Force Office of Scientific Research (AFOSR) grant no. FA9550- 19- 1-0278. R.B. acknowledges that this project has received funding from the European Union's Horizon 2020 Research and Innovation Programme under Marie Skłodowska-Curie Grant Agreement no. 898571. A.A. acknowledges financial support from the Kuwait Foundation for the Advancement of Sciences (KFAS). A.X.C. acknowledges financial support from a UC President's Dissertation Year Fellowship. L.L.B. acknowledges support from a National Science Foundation Graduate Research Fellowship (NSF GRFP) under grant no. DGE-2038238 and funding from the Achievement Rewards for College Scientists (ARCS) Foundation. N.R. and R. Rouw acknowledge financial support from the Dutch Research Council (NWO) under grant 406.21. GO.021. S.M.R. and S.A.D. were partially supported by the National Institutes of Health primarily through award no. NIBIB DP2-EB029757 (to S.A.D.) and in part by the BRAIN Initiative NIH grants R01NS123655 (to S.A.D.) and UG3NS123723 (to S.A.D.). This research was supported in part by the NSF through the UC San Diego Materials Research Science and Engineering Center (DMR 2011924). The authors acknowledge the use of facilities and instrumentation at the UC Irvine Materials Research Institute (IMRI), which is supported in part by the National Science Foundation through the UC Irvine Materials Research Science and Engineering Center (DMR-2011967). This work was performed in part at the San Diego Nanotechnology Infrastructure (SDNI), a member of the National Nanotechnology Coordinated Infrastructure, which is supported by the National Science Foundation (grant ECCS-1542148). All human participant testing was conducted in accordance with the ethical guidelines with the approval of the Institutional Review Board (#805425) of UC San Diego. **Author contributions:** Conceptualization: R.B., A.A., and D.J.L. Methodology: R.B., A.A., N.R., A.X.C., R. Ramji, Y.Q., T.R., T.K., A.N., J.C., S.E., L.L.B., S.M.R., S.A.D., and R. Rouw. Investigation: R.B., A.A., and N.R. Visualization: R.B., A.A., N.R., and T.R. Funding acquisition: D.J.L. Project administration: R.B., A.A., and D.J.L. Supervision: D.J.L. Writing—original draft: R.B., A.A., and N.R. Writing—review and editing: R.B., A.A., N.R., A.X.C., D.P.F., and D.J.L. **Competing interests:** S.A.D. has competing interests that are not related to this work, including equity in Cortical Sciences Inc. that concerns the commercialization of brain recording and stimulation electrodes, and is a paid consultant to MaXentric Technologies. The other authors declare that they have no competing interests. **Data and materials availability:** All data needed to support the conclusions of this manuscript are included in the main text or Supplementary Materials. The code to generate statistics and visualizations is available at DOI 10.5281/zenodo.11177411.

Submitted 18 August 2023
Accepted 16 May 2024
Published 12 June 2024
10.1126/scirobotics.adk3925

Correction (15 April 2025): Grant information for DMR 2011924 was omitted in the final published version. The Funding subsection of the Acknowledgments has been updated. The other data and the conclusions are not affected.

Science Robotics

Conductive block copolymer elastomers and psychophysical thresholding for accurate haptic effects

Rachel Blau, Abdulhameed Abdal, Nicholas Root, Alexander X. Chen, Tarek Rafeedi, Robert Ramji, Yi Qie, Taewoo Kim, Anthony Navarro, Jason Chin, Laura L. Becerra, Samuel J. Edmunds, Samantha M. Russman, Shadi A. Dayeh, David P. Fenning, Romke Rouw, and Darren J. Lipomi

Sci. Robot. **9** (91), eadk3925. DOI: 10.1126/scirobotics.adk3925

Editor's summary

Most haptic devices rely on mechanical actuators to stimulate the skin but are limited in range. Alternatively, electrical stimulation of mechanosensory neurons can be perceived as a mechanical force but often requires high currents and leads to unwanted effects, such as pain. Blau *et al*. developed an electrotactile device made from a conductive block copolymer in a serpentine shape that exhibited microscopic conformability with the skin. When tested on human participants, the device provided stimulation at very low currents and could toggle between pressure and vibration by changing the signal frequency. Safe and reliable electrotactile stimulation is a promising development for haptic devices such as human-machine interfaces and prosthetics. —Melisa Yashinski